Check for updates

Protein-coated nanoparticles exhibit Lévy flights on a suspended lipid bilayer†

Jean-Baptiste Fleury, [ID] *[a] Vladimir A. Baulin[b] and Xavier Le Guével [ID] [c]

Lateral diffusion of nano-objects on lipid membranes is a crucial process in cell biology. Recent studies indicate that nanoparticle lateral diffusion is affected by the presence of membrane proteins and deviates from Brownian motion. Gold nanoparticles (Au NPs) stabilized by short thiol ligands were dispersed near a free-standing bilayer formed in a 3D microfluidic chip. Using dark-field microscopy, the position of single NPs at the bilayer surface was tracked over time. Numerical analysis of the NP trajectories shows that NP diffusion on the bilayer surface corresponds to Brownian motion. The addition of bovine serum albumin (BSA) protein to the solution led to the formation of a protein corona on the NP surface. We found that protein-coated NPs show anomalous superdiffusion and that the distribution of their relative displacement obeys Lévy flight statistics. This superdiffusive motion is attributed to a drastic reduction in adhesive energies between the NPs and the bilayer in the presence of the protein corona. This hypothesis was confirmed by numerical simulations mimicking the random walk of a single particle near a weakly adhesive surface. These results may be generalized to other classes of nano-objects that experience adsorption–desorption behaviour with a weakly adhesive surface.

1. Introduction

In the context of the development of the next generation of therapeutic nanomaterials, the prediction of nanoparticle (NP) trajectories and their behaviour on the cell surface is considered the Holy Grail.[1,2] Determining how engineered NPs would escape or enter cells in a complex cellular environment that can interact on the NP surface is of great importance and would impact their efficacy for drug delivery, antibacterial action, or the ability to hide from the immune system.[1,3,4] For instance, gold nanoparticles (Au NPs) are relevant carriers for delivering biomolecules of interest into living cells, as antibacterial agents or as a diagnostic platform[5–8] due to their inertness and the ability to tailor their size, shape, surface chemistry and to exploit their unique interaction with light for imaging, sensing and phototherapy purposes.[5–9] When NPs approach the surface of a living cell, they can attach to it and move along the cell surface in a complex manner.[1] This phenomenon may determine their fate within the cellular environment. Depending on NP motion, they can cluster on the cell surface, be internalized, or return to the host phase.[10]

With recent developments in microscopy techniques, it is now possible to visualize individual NPs and track the diffusion of these NPs at the surface of bilayers.[11] The resulting trajectories can occasionally be characterized by a classical two-dimensional random walk,[12] but are often reported as anomalous diffusion, where their diffusive behaviour evolves over time.[13–18] The physical origins of such anomalous diffusion is still under debate.[13–20] The presence of obstacles,[21,22] heterogeneous diffusion,[23] non permanent binding,[24] diffusing diffusivity,[25] hopping,[26] excluded area fractions[20] and compartmentalization[19] are commonly considered to be possible origins. All these effects highlight the pivotal role of biomolecules present in the cell membrane (such as transmembrane proteins), as sources of anomalous diffusion. However, in these studies, the possible role of biomolecules present outside the cell is not considered a possible source for such anomalous behaviour. One example of biologically relevant biomolecule that can affect the interaction of NPs with lipid membranes, is the class of water-soluble proteins.[27–29] A protein corona is a protein layer that is adsorbed on the NP surface.[27] The presence of the protein corona modifies the surface properties of the NPs, which influence the interactions between NPs and cells, such as cellular recognition.[30–32]

[a]Universitat des Saarlandes, Experimental Physics and Center for Biophysics, 66123 Saarbruecken, Germany. E-mail: jean-baptiste.fleury@physik.uni-saarland.de
[b]Departament Química Física i Inorgànica, Universitat Rovira i Virgili, Marcel.li Domingo s/n, 43007 Tarragona, Spain
[c]Cancer Targets & Experimental Therapeutics, Institute for Advanced Biosciences (IAB), University of Grenoble Alpes - INSERM U1209 - CNRS UMR 5309-38000 Grenoble, France
†Electronic supplementary information (ESI) available. See DOI: https://doi.org/10.1039/d2nr01339h

In this work, we investigated the influence of the protein corona on the diffusion of 75 nm and 100 nm Au NPs stabilized by ligands in contact with a large, horizontal free-standing lipid bilayer formed on a 3D microfluidic chip.[33] To this end, we observed the motion of individual water-soluble Au NPs near a lipid bilayer using dark-field microscopy.[34,35] We, also, studied the motion of NPs coated with a protein corona that is only composed of bovine serum albumin (BSA)[36] (see Methods section). We demonstrated that, in the absence of a protein corona, NPs exhibit Brownian motion, while in the presence of a protein corona, NPs exhibit Lévy flight.[37] We suppose that these results may be generalized to many other classes of nano-objects that experience adsorption–desorption around a weakly adhesive surface.

2. Results and discussion

2.1. Au NP characterization

We prepared batches of Au NPs with narrow size distributions (CV < 5%) of 75 nm and 100 nm as confirmed by Transmission Electron Microscopy (TEM) (Fig. S1†). We used a previously described protocol[9] to functionalize the Au NP surface with either a short thiolated ligand containing a terminal acid group (MHA) or with a slightly hydrophobic modified-bidentate sulfobetaine zwitterionic (ZwBuEt).[38] We determined the hydrodynamic diameter and the surface charge of these four samples: $Au_{75}NP$-MHA, $Au_{75}NP$-ZwBuEt, $Au_{100}NP$-MHA, and $Au_{100}NP$-ZwBuEt before and after incubation with BSA (Table S1†). We measured a negatively charged surface for Au NPs coated with MHA ($\zeta \approx 20$ mV) and with ZwBuEt ($\zeta \approx 7$ mV) which were not strongly influenced by the NP size or after BSA incubation. The hydrodynamic diameter of the 75 nm and 100 nm Au NPs, determined by DLS, increased in the same range between 10 and 30 nm in the presence of BSA independent of the NP core size and the nature of the ligands. This finding is consistent with a previous study that examined a series of Au NPs-citrate of different sizes where a protein corona thickness in the same order for the 80 nm and 100 nm particle size.[39] The thickness of the protein corona can be estimated to be a maximum of three layers of protein considering the globular shape of BSA (3 nm × 4 nm × 7 nm). We did not notice any aggregation of the different NPs after BSA incubation over time indicating the good stability of these coated Au NPs.

2.2. Adsorption of Au NPs on a free-standing lipid bilayer

To measure the adsorption energy between Au NPs and a free-standing lipid bilayer, Au NPs coated with ligands of different hydrophobicity were used because of their different interactions and adhesion on the lipid bilayer; the MHA ligand is more hydrophobic than the ZwBuEt ligand considering their log P value.[9] While both types of NPs present good colloidal stability in aqueous solution, their ligands affect the global surface properties of NPs, thereby affecting NP adsorption, as previously demonstrated.[38]

A free-standing bilayer was formed as described in the Methods section. $Au_{100}NPs$, at a low concentration ($c \approx 20$ μg ml^{-1}), were dispersed around the bilayer by means of microfluidic pumps according to the schematic (Fig. 1). These Au NPs can be easily detected over time on the bilayer surface by dark-field microscopy.[9,34,35] Brownian analysis of the NPs confirmed that the NPs were individual (see Table 1). Thus, the NPs did not aggregate into clusters and moved freely around the bilayer. Surprisingly, a small fraction of these Au NPs also adhered to the bilayer and were stacked permanently at the surface. They could be easily distinguished from other free NPs, as they were drastically slower than unbound NPs, and could be automatically sorted out using image analysis. Over time, adsorption from the bulk material resulted in an increasing number of surfaces covered by adsorbed NPs. Due to the larger size of the NPs compared to the lipid bilayer thickness (≈ 5 nm), we can safely assume that these immobile NPs were not inserted into the bilayer core and stayed on the bilayer surface.[9,38,40] This analysis provides the NP adsorption rate at the surface of the bilayer.

This lipid bilayer corresponds to a potential well that holds the particles, and that they have to cross otherwise they are irreversibly trapped. Indeed, we did not observe any spontaneous desorption of these NPs after they were irreversibly adsorbed. Thus, this process corresponds to irreversible adsorption with only a one way adsorption constant taken into account. The energy barrier of this irreversible adsorption can be estimated through the Arrhenius expression:[41,42]

$$k_{ads} = k_1 e^{-\frac{\Delta G}{k_B T}} \tag{1}$$

where k_1 is a constant, k_B is the Boltzmann constant, T is the temperature and ΔG is the free energy difference that controlled the adsorption. For the tested bilayer composition, we measured a potential barrier of ≈ 9.5 $k_B T$ for 100 nm Au NPs stabilized by ZwBuEt ligands and with a more hydrophobic ligand MHA, and measured a potential barrier of ≈ 11 $k_B T$ (see Fig. 2). This difference in energy, and thus a difference in adsorption rate, demonstrated that adsorption is influenced by the ligand hydrophobicity.[38] It is noteworthy that the difference in the free energy barrier is not significant for smaller particle sizes (75 nm diameter) and is independent of the nature of the ligands, probably due to the NP curvature and the density of ligand grafting. The addition of bovine serum albumin (BSA) to a solution of Au NPs in phosphate saline buffer (PBS) led to the rapid formation of a protein corona surrounding the Au NPs (see Methods).[35,38] Using BSA-NPs, the measured aggregation rate observed by dark field microscopy dropped dramatically (Fig. 2B). This observation demonstrated that the BSA coating on the NP surface strongly increased the energy barrier controlling NP adsorption. Although it is difficult to accurately determine this energy barrier, it is estimated to be above 30 $k_B T$.[40]

When the NPs are coated with BSA, there is no irreversible NP adsorption on the bilayer surface (Fig. 2B). This is a regime of reversible adhesion, where the NPs are touching and leaving
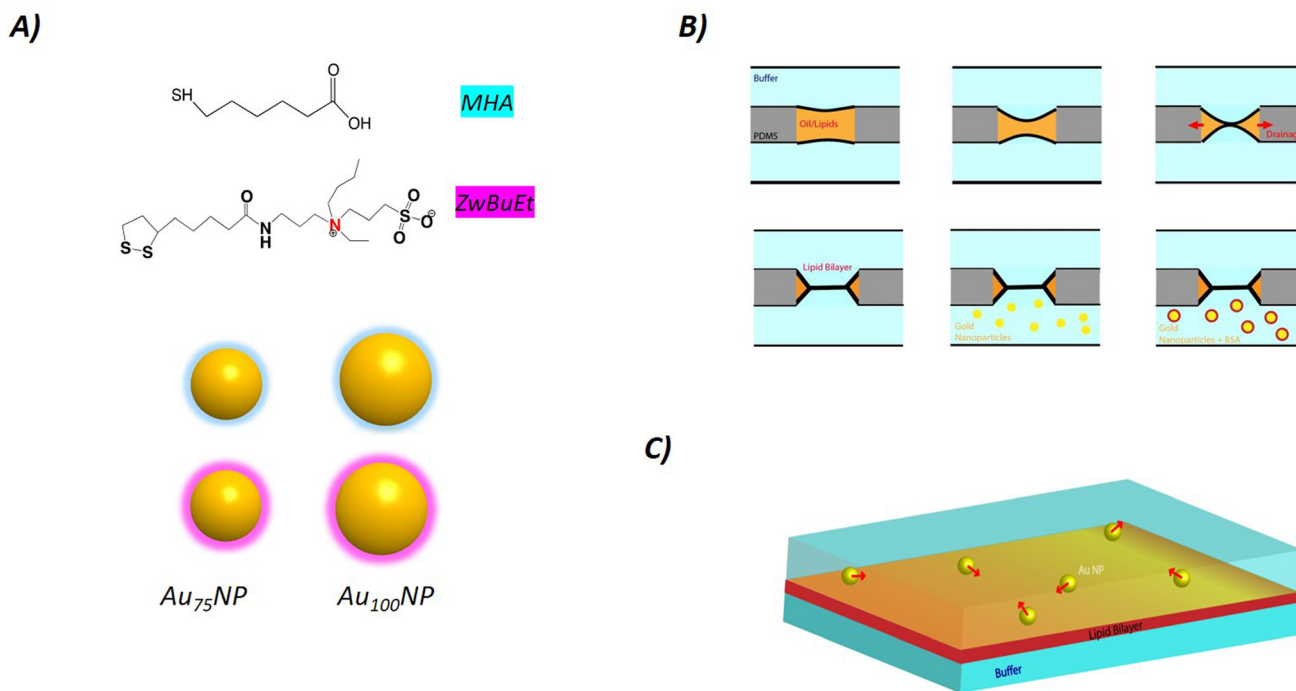
Fig. 1 (A) Molecular formula of the ligands: mercaptohexanoic acid (MHA) and modified-bidentate sulfobetaine zwitterionic molecule (ZwBuEt), which are coated on Au NPs of two different sizes (75 nm; 100 nm). (B) Schematic view of the formation of the lipid bilayer. First, a buffer-oil-buffer sandwich is formed by means of microfluidic pumps. Then, the oil phase is drained spontaneously by the chip material (PDMS, see Method) until a lipid bilayer is formed. Then, Au NPs are dispersed with or without proteins coronas around the bilayer. To prevent sedimentation of the gold nanoparticles onto the bilayer, Au NPs were dispersed in the bottom channel. (C) Schematic 3D-view of the lipid bilayer with Au NPs diffusing on the surface of the bilayer. The NPs are shown above the bilayer for better visualization.

Table 1 Measured diffusion coefficient of Au NPs (with ZwBuEt and MHA ligands) on bilayer surface D, and the thickness of the protein corona ζ

Size (nm)	100	100 + BSA	75	75 + BSA
D_{ZwBuEt} ($\mu\text{m}^2\ \text{s}^{-1}$)	5.6	4.8	5.5	4.4
D_{MHA} ($\mu\text{m}^2\ \text{s}^{-1}$)	4.8	4.1	4.7	3.9
ζ_{ZwBuEt} (nm)	—	16	—	25
ζ_{MHA} (nm)	—	17	—	25
$\Delta G'_{\text{ZwBuEt}}$ ($k_B T$)	—	0.2–3	—	0.2–3
$\Delta G'_{\text{MHA}}$ ($k_B T$)	—	0.2–3	—	0.2–3

the bilayer reversibly. In this regime, the NPs are also in the presence of an energy barrier that is provided by the adsorption–desorption rates. The adsorption rate k_{ads} and desorption rate k_{des} are connected as follows $k_{\text{ads}}/k_{\text{des}} = \text{e}^{-\frac{\Delta G'}{k_B T}}$ with $\Delta G'$ is the adsorption–desorption energy barrier.[41] Thus, using experimental movies, it is possible to evaluate the range of the adsorption–desorption barrier of 0.2–3 $k_B T$ for 100 nm coated with BSA (for both ligands). This value of adsorption–desorption energy barrier is used later in our Langevin simulations.

2.3. Diffusion of Au NPs at the bilayer surface with and without BSA

First, we dispersed Au NPs around a formed free-standing lipid bilayer. The motion of these Au NPs at the surface of the

bilayer was recorded for two Au NP sizes (100 nm, 75 nm) and with the two coatings (MHA, ZwBuEt). Notably, Au NP trajectories cannot be recorded for times longer than few minutes. It is very likely that at longer times Au NPs either detach from the bilayer and return to the bulk, or simply stick to the bilayer. As described in the previous section, if some NPs may become quasi-immobile. If so they were not more considered and were sorted out numerically by their speed. Thus, the corresponding Au NP trajectories and mean square displacements (Fig. 2A), were automatically extracted[43] using numerical methods (see Methods section).[44]

We can approximate the studied Au NP motion on a bilayer surface, as a two-dimensional motion. In 2D, the mean square displacement is represented by: $\langle r^2 \rangle = <|r(t) - r_0|^2> = \frac{1}{N}\sum_{i=1}^{N}|r^i(t) - r_0^i|^2$, where $r(0) = r_0$ is the reference position of particle i as a function of time t. It provides an estimate for the corresponding diffusion constant D of diffusing Au NPs,

$$\langle r^2 \rangle = 4Dt \tag{2}$$

The measured diffusion constants D are summarized in Table 1 for all different types of NP sizes and ligands, used in this study. The extracted random motion presents Brownian diffusion, as the mean square displacement $\langle r^2 \rangle$ is linear with time t (see eqn (2)). However, the diffusion constants were
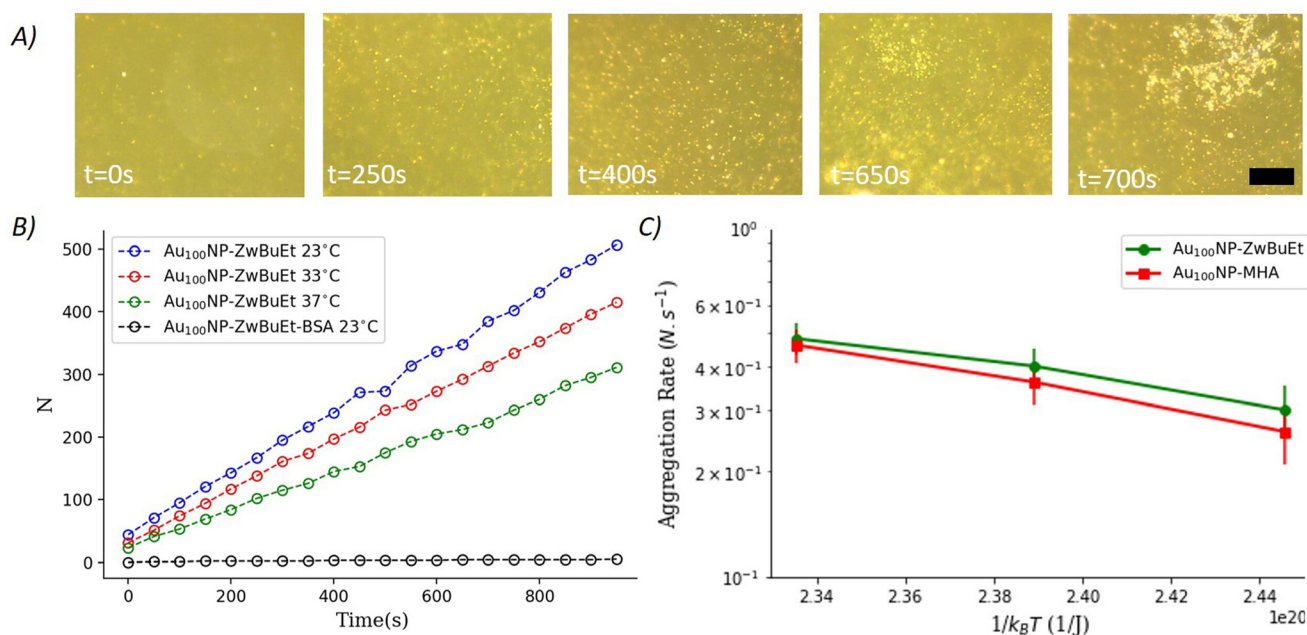
Fig. 2 (A) Micrographs of 100 nm gold nanoparticles (Au$_{100}$NP-ZwBuEt) observed by far-field microscopy (scale bar corresponds to 40 μm). (B) Micrograph image provides the number of Au$_{100}$NP-ZwBuEt adhered to the lipid bilayer as a function oftemperature. Black dots represent the number of Au$_{100}$NP-ZwBuEt coated with BSA that adhered to the bilayer at 23 °C. (C) Semi-log plot of Au$_{100}$NP-ZwBuEt aggregation rate N.s^{-1} as a function of thermal energy $1/k_BT$, for two different types of ligands. The corresponding adsorption energies were calculated to be ≈9.5k_BT for Au$_{100}$NP-ZwBuEt and ≈ 11 k_BT for Au$_{100}$NP-MHA. Experimental points are the result of averaging 10–20 exps.

≈ 1–3 times smaller than the expected values predicted from the Stokes–Einstein equation.[45] It is important to note that this discrepancy has not come from cluster formation, since dynamic light scattering (DLS) measurements show that the Au NPs in the bulk are stable individual particles (Table S1†). However, this difference may come from the difficulty of quantifying friction between the bilayer surface and the NPs.[46–48] Considering friction for the case of NPs moving at the bilayer surface, the corrected Stokes–Einstein equation can be expressed as:[46–48]

$$D = \frac{1}{c(\lambda)}\frac{k_BT}{4\pi\eta_m} \quad (3)$$

where $c(\lambda)$ is a dimensionless parameter and η_m is the membrane viscosity. There are considerable discrepancies between the reported membrane viscosity η_m from the motion of particles strongly attached to a lipid bilayer.[46,49,50] We cannot disprove that the NPs start to cluster while moving along the bilayer surface. Thus, it is not possible to clearly identify the physical origin behind the expected theoretical diffusion constant and the measured experimental diffusion constant. Interestingly, these results are barely affected by the type of ligand covering the nanoparticles (see Table 1).

We repeated these experiments with the same NPs, but incubated them with BSA to generate a protein corona (see Methods). The statistical analysis of the recorded particle trajectories revealed that the diffusion of the BSA-NPs was anomalous over time. These results were presented in Fig. 3. The mean square displacement ⟨r^2⟩ presented a linear behaviour

as a function of t, at a short time (before a few seconds). However at longer times, the mean square displacement ⟨r^2⟩ varied and presented a linear behaviour as a function of $t^{1.2}$, which is a superdiffusive behaviour (see Fig. 3).[45,51] This behaviour was particularly visible for the 75 nm NPs and independent of the nature of the ligands. The difference in the behaviour of BSA-NPs could be explained by the weak adhesive interaction between the BSA-NPs and the lipid bilayer in the presence of the protein corona. In contrast, the stronger adsorption energy between pure NPs and the bilayer may hinder pure NP escape. Thus, this superdiffusion may originate from the corona that shields the attractive bilayer interactions and thus escapes the bilayer surface more easily.[51]

This particle-hopping hypothesis is similar to a Lévy-flight diffusion model and thus can be tested.[52] For this purpose, we extracted the NP relative displacement $r(t)$ (with $r_0 = 0$) frequency for thousand of single NP trajectories (see Fig. 4A). It appeared that this distribution respected a Lévy-stable probability density function defined as

$$f(r) = \frac{1}{\sqrt{2\pi r^3}}\exp\left(-\frac{1}{2r}\right) \quad (4)$$

for $r \geq 0$ (see Methods and ref. 53 for details). This successful fitting confirms that BSA-NPs exhibit Lévy flight along the bilayer surface. We suppose that the emergence of Lévy flights occur for NPs weakly adsorbed on alipid bilayer, while NPs strongly adsorbed onto a lipid bilayer respected typical Brownian motion. Interestingly, Bouchaud and Daoud showed that the 2D projection of a linear polymer weakly adsorbed on
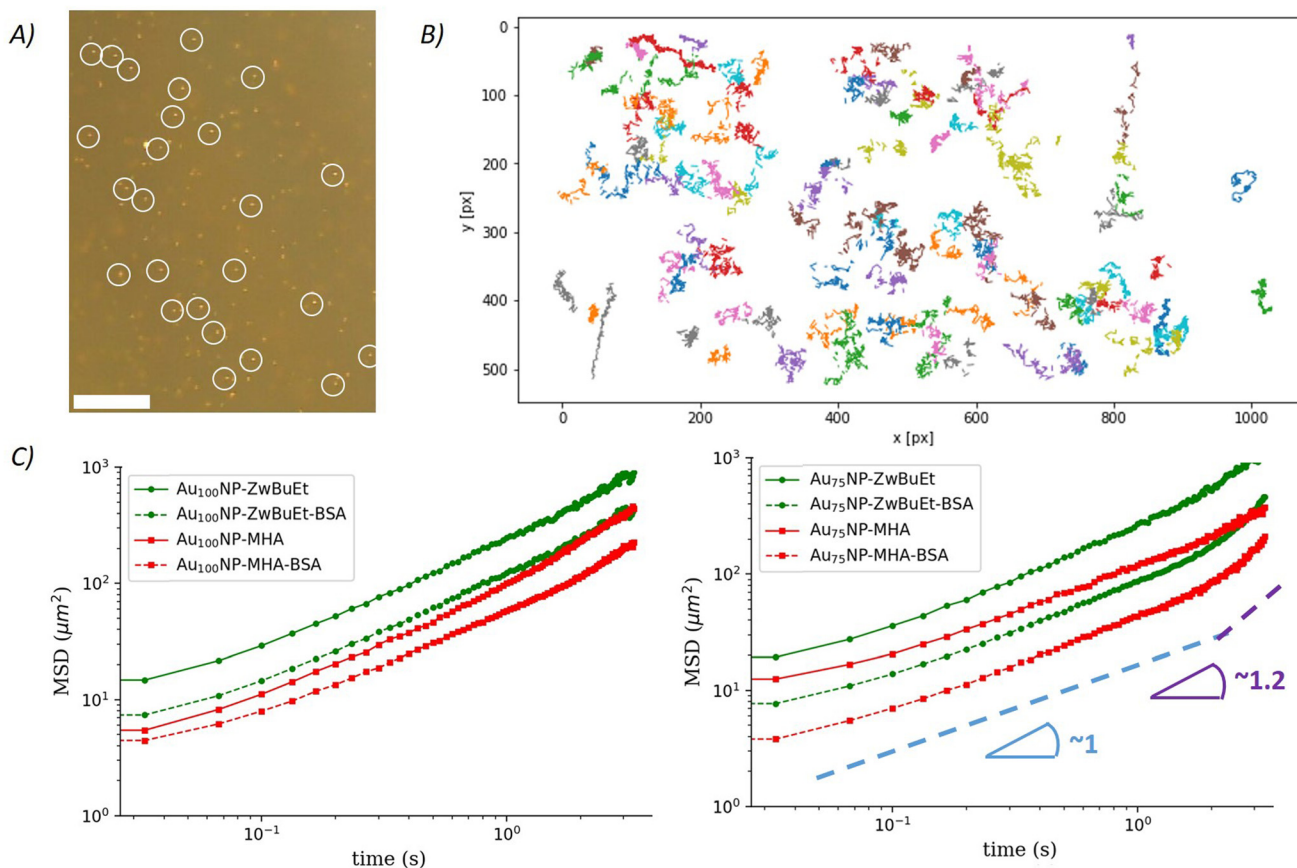
Fig. 3 (A) A micrograph depicting 100 nm Au NPs functionalized with ZwBuEt ligand, observed under dark field (length bar correspond to ≈ 60 μm). The considered NPs are identified with non-overlapping white circles. (B) Hundred of trajectories of 40 s of 100 nm gold nanoparticles functionalized with ZwBuEt ligand. Trajectories were presented after drift removal and trajectories shorter than 100 points were automatically filtered. (C) The extracted mean square displacement $\langle r^2 \rangle$ as a function of time t in log−log scale. Left panel, is presenting the results for 100 nm particles with ZwBuEt and MHA ligands, with and without BSA. Right panel, is presenting the results for 100 nm particles with ZwBuEt and MHA ligands, with and without BSA. Two time t^α exponents α are schematically plotted with the two dash lines without dots.

a surface is equivalent to a node-avoiding Lévy flight, while the projection of a strongly adsorbed linear polymer is equivalent to Brownian motion.[54] As a test, we simulated 3D walks of a single particle based on a 3D-Langevin equation (Methods, Fig. 4B–D). This particle is moving under a stochastic process, near a solid surface. If the particle has no adhesive interaction with the surface, the corresponding motion is a 3D Brownian walk (Fig. 4). In case where there is a strong adhesive interaction between the surface and the particle (*e.g.* more than a few $k_B T$, see Methods), the calculated motion is a quasi-2D motion. In the case, there is a weak adhesive interaction between the surface and the particle (*e.g.* in the range of 0.2–0.5$k_B T$, see Methods), the particle is hopping along the surface. These results demonstrate that under weak adhesion energies, a particle may jump along the surface in a similar way than Lévy flights[26,37]. These Lévy flights may indicate the vicinity of a critical point.[55] In the case of NP interactions with a lipid bilayer, this critical point could be associated with the adsorption–desorption transition of an NP to the bilayer and characterized by the balance of attraction and repulsion. The

critical point is thus defined by a threshold value of the adsorption energy between the NP and the bilayer. Hereby, we could observe that the NP relative random motion is larger when the NP position is not exactly in contact with the bilayer, and smaller when the NP position is close to the bilayer (see ESI†).

Interestingly, the ratio between the diffusion constant of pure NPs and BSA coated NPs is:

$$\frac{D}{D_{\text{BSA}}} \approx \frac{R_{\text{BSA}}}{R},$$

(5)

it provided an estimation of the protein corona layer thickness ζ. It appeared that for 100 nm Au NPs the corona protein layer was $\zeta_{100\ \text{nm}} \approx 16$ nm for the ZwBuEt ligand and $\zeta_{100\ \text{nm}} \approx 17$ nm for the MHA ligand. For 75 nm Au NPs the corona protein layer was $\zeta_{75\ \text{nm}} \approx 25$ nm for ZwBuEt and $\zeta_{75\ \text{nm}} \approx 20$ nm for MHA ligand. Thus, the protein corona layer thickness ζ corresponded to a BSA layer, with a single BSA protein having a size of ≈ 7.1 nm.[56,57] These results are, in the order of
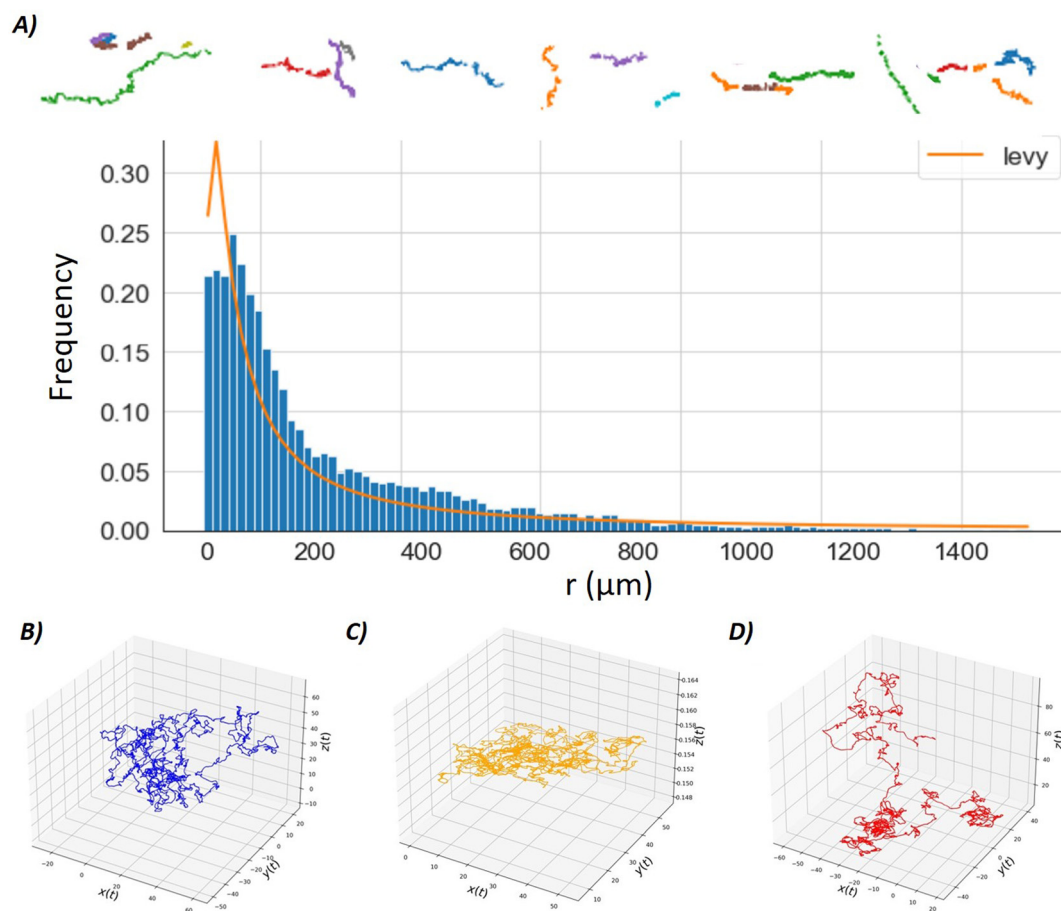
Fig. 4 (A) Frequency of several thousand NP relative displacements $r(t)$, centred on their initial position ($r(t = 0) = 0$) for BSA-coated NP (75 nm, ZwBuEt ligand). This histogram is fitted by a Lévy-stable distribution (see eqn (4)). Above row: A few Levy-flight trajectories are plotted and could be directly compared with Brownian trajectories plotted in Fig. 3B. Lower panel, 3D-trajectories of as single particle calculated from the Langevin equation by numerical simulations (see Methods). (B) A blue particle moves around a solid surface with no adhesive attraction between the surface and the particle (see Methods). The corresponding motion is a standard Brownian motion. (C) An orange particle moves around a solid surface with a strong adhesive attraction between the surface and the particle (see Methods). The corresponding motion is quasi 2D only. (D) A red particle moves around a solid surface with a weak adhesive attraction between the surface and the particle (see Methods). In that case, the particle is hopping along the surface.

magnitude, consistent with our DLS measurements (Table 1 and ESI†) and literature.[39,58]

3. Conclusion

In this study, we explored the effects of a BSA coating on the diffusive properties of Au-NPs moving on the surface of a free-standing bilayer by tracking single NPs by dark field microscopy. The diffusive motion of ≈100 nm Au NPs with two different surface chemistry was recorded with and without protein coating. In the absence of proteins, individual Au NPs showed a typical Brownian motion. The extracted diffusion constant of Au NPs near the bilayer surface was slightly lower than the diffusion constant for the particles in the bulk, which might be due to the complex interaction and friction between the bilayer and the NPs. A slight change in the diffusion con-

stant accompanied by a superdiffusive motion for BSA coated Au NPs was observed after a few seconds (Fig. 3), indenpendent of the size and nature of the ligands tested in this study. The origin of this superdiffusive behaviour is attributed to the weak adhesive interaction between BSA-coated Au NP and the bilayer. The trajectory analysis reveals that the BSA-coated NPs follow Lévy-flight distribution, which confirms the nature of a particle-hopping motion (as expected for Lévy flights). This conclusion was also confirmed by performing simulations based on a 3D-Langevin equation in the presence of an adhesive surface.

Protein corona strongly affects the adsorption energies between a model cell membrane and Au NPs, which are related to the rates of adsorption and desorption. Lévy flight diffusion can be a manifestation of a vicinity to the critical point of the adsorption–desorption transition for the NPs at the bilayer. Finally, our method provides a new experimental

tool to estimate protein layer thickness. The thickness of the protein layer can strongly affect the NP motion on a surface and even induce superdiffusion. However, a limitation of this new experimental method is the limited precision for small NPs. Certain universality of the mechanism behind Lévy-flight diffusion of nanoparticles and modulation of this behaviour with protein corona suggests generalizations to other types of nanoparticles and highlights the role of protein corona in interaction with lipid bilayers near adsorption–desorption transition.

4. Materials and methods

4.1. Molecules and proteins

The buffer is composed of phosphate buffered saline (PBS) at PH 7.4 (Sigma-Aldrich). 1,2-Dioleoyl-*sn-glycero*-3-phosphocholine (DOPC) and 1,2-dioleoyl-*sn-glycero*-3-phosphoethanolamine (DOPE) were purchased from Avanti Polar Lipids. Squalene oil is from Sigma Aldrich. The Bovin Serum Albumine (BSA) protein was purchased from Sigma Aldrich. The NPs are incubated ≈30 minutes with BSA, at the concentration indicated in the manuscript, before being injected into the µchip.

4.2. Gold nanoparticle fabrication

Gold nanoparticle (Au NP). Au NPs of 75 and 100 nm were synthesized using slightly modified protocols described by Perrault *et al.*,[59] as follows: citrate gold seeds were prepared by adding 300 µL of $HAuCl_4$. $3H_2O$ (1% W/V) to 30 mL of deionized water and brought to boiling point. Then 900 µL sodium citrate trihydrate (1% W/V) was added and solution was stirred for 30 min before cooling at room temperature. A fresh growth solution of 75 nm Au NPs was made by adding 100 µL $HAuCl_{43}H_2O$ (1% W/V) to 9.5 mL of water. After adding 100 µL of gold seeds to the growth solution, 100 µL of hydroquinone (30 mM) and 22 µL of sodium citrate trihydrate (1% W/V) were added at the same time. Solution changed colour quickly from colourless to purple-reddish and was kept stirring for 1 h to complete the reaction. To obtain a batch of 100 nm Au NPs, we only reduced the volume of gold seeds to 75 µL during this synthesis step. Both 100 nm and 75 nm Au NPs were washed 3× and resuspended in MilliQ H_2O at 100 µg Au mL^{-1}.

Gold nanoparticle coating. In 10 mL of Au NP solution (100 µg Au mL^{-1}), 40 µL of NaOH (1 M) was added followed by 100 µL of ZwBuEt (0.5 mM) or MHA (0.5 mM) and stirred for another 6 h. ZwBuEt-coated Au NPs and MHA-coated Au NPs were washed 3 times in Milli-Q H_2O using a centrifugation method (10 000 rpm for 20 min) to remove excess free thiol molecules. Sols were stored in DI H_2O at 1 mg Au mL^{-1}. Sulfobetaine presents a crucial advantage over cysteine coatings, as it does not contain any primary amines or carboxylic acids, is chemically inert, highly stable in high salinity or over a wide pH range, can be easily functionalised and displays reduced opsonization in the presence of high serum content.[9,38]

4.3. Gold nanoparticles incubated with bovine serum albumine (BSA)

Au NPs of different sizes (75 nm, 100 nm) and coated with MHA or ZwBuEt ligands were dispersed in an aqueous solution of BSA (50 mg.mL^{-1}) during 1 hour at 37 degrees. Au NPs were then centrifuged twice at 10 000 rpm for 5 min to remove the free BSA and the NPs were resuspended in water before use.

4.4. Gold nanoparticle characterization

High-resolution transmission electron microscopy (HRTEM) images were measured on a JEOL 2010 LaB$_6$ microscope operating at 200 kV with a 0.19 nm point-to-point resolution after the deposition of the Au NPs on a Formvar carbon grid. The images of at least 100 NPs collected were analyzed with ImageJ software. DLS and zeta potential measurements of the different Au NP samples were performed on a Zetasizer (Malvern). Measurements were performed in triplicate at 25 °C. For water, 1.33 and 0.89 mPa s were taken as the refractive index and viscosity values, respectively.

4.5. Horizontal lipid bilayer formation with microfluidics

A 3D microfluidic chip was obtained from the fabrication technique detailed in ref. 9, 33, 35 and 60. Then the chip was obtained by curing PDMS (polydimethylsiloxane) at 60 °C for 3 h in an oven, Sylgard 184, purchased from Dow Corning. The solidified PDMS chip is then bonded to a glass substrate after plasma treatment (plasma cleaner from Diener). After connecting the 3D-chip with tubings to homemade computer-controlled microfluidic pumps, the chip was filled with an oil–lipid mixture (with a 2 mg ml^{-1} lipids concentration). After carefully injecting buffers into the bottom and top microchannels, two liquid fingers were separated by an thin oil film, which was spontaneously drained by the PDMS porous material. As the two water/oil interfaces are covered by a lipid monolayer, they red spontaneously form a free standing lipid bilayer at a contact. Finally, bilayer formation was demonstrated by electrophysiological and optical investigations.[9,33,35,43,60] The motion over time of the dispersed Au NPs near the bilayer was monitored by dark-field microscopy (Leica DM2700 microscope). In this article, the lipid composition of the bilayer is DOPC/DOPE (70 : 30 in molar ratio). The measured relative lateral pressure for this bilayer is ≈ 3 mN m^{-1}, the measurement method is detailed in ref. 61. The chip is maintained at constant temperature, under a Teflon chamber, to avoid temperature drift.

4.6. Image analysis and statistical Analysis

Movies are analysed using Python and Python libraries: the NPs trajectories and MSD are extracted using TrackPy.[44] NP relative displacements are extracted using Pandas and automatically fitted with a Lévy-stable distribution using Seaborn and SciPy libraries. To avoid statistical artefacts when measur-

ing the NP relative displacement, we consider only particles that stay inside the region of interest. The distribution for a Lévy stable distribution is the following characteristic function:

$$\phi(t, \alpha, \beta, c, \mu) = e^{it\mu - |ct|^{\alpha}(1 - i\beta \, \text{sign}(t)\Phi(\alpha, t))} \tag{6}$$

with

$$
\begin{aligned}
\Phi &= \tan\left(\frac{\pi\alpha}{2}\right), \quad \text{if } \alpha \neq 1 \text{ and} \\
\Phi &= -\frac{2}{\pi}\log|t|, \quad \text{if } \alpha = 1
\end{aligned}
\tag{7}
$$

The corresponding Lévy probability density function is

$$f(x) = \frac{1}{2\pi}\int_{-\infty}^{+\infty} \phi(t)e^{-ixt}dt. \tag{8}$$

In the case, $r \geq 0$, $\alpha = 1/2$ and $\beta = 1$, we obtained the Lévy probability density function employed in this manuscript[53]

$$f(x) = \frac{1}{\sqrt{2\pi x^3}}\exp\left(-\frac{1}{2x}\right). \tag{9}$$

4.7. Simulation of a Brownian particle based on a 3D Langevin equation

The Langevin equation was used to describe the motion of a Brownian particle due to its stochastic nature. The equation is derived directly from Newton's second law ($F = ma = m\mathrm{d}v(t)/\mathrm{d}t$), taking into account friction through a random force due to the ambient molecule collisions $m\mathrm{d}v(t)/\mathrm{d}t = -\gamma v(t) + \eta(t)$, where m is the mass of a nanoparticle, γ is the friction, $v(t)$ is the nanoparticle velocity, $x(t)$ is the nanoparticle position and $\eta(t)$ is the noise/stochastic force. These parameters are fixed to $m = 1$, $\gamma = 1$, $k_B = 1$, $T = 300$. The noise term satisfies the conditions $\langle\eta(t)\rangle = 0$ and $\langle\eta_i(t)\eta_i(t)(t')\rangle = A\gamma\delta_{ij}\delta(t - t')$, where A is a positive constant, δ_{ij} is the Kronecker symbol and δ the Dirac Delta function. The attractive adhesion energy of the nanoparticle to the surface is introduced according to ref. 62. Depending on the adhesion strength, the particle motion could be completely free (when this term is zero), totally confined in 2D (strong adhesion, energy barrier above a few $k_B T$) or hopping motion on the surface (weak adhesion, in the range of 0.2–$0.5 k_B T$). Example of trajectories are displayed in Fig. 4B–D, other trajectories with velocities are available in ESI.† It shows that the Brownian motion can also be anomalous as in ref. 26. This simulation is performed using MATLAB code described in ESI† of ref. 63 and converted into Python. More details are provide in the ESI.†

Author contributions

J.-B. F. designed and performed the experiments and the numerical simulations. V. A. B and J. B.-F. performed the image analysis. X. L. synthesized and characterized the nanoparticles. All the authors discussed the results and wrote the article.

Conflicts of interest

The authors declare no conflicts of interest.

Acknowledgements

References

1 M. J. Mitchell, M. M. Billingsley, R. M. Haley, M. E. Wechsler, N. A. Peppas and R. Langer, *Nat. Rev. Drug Discovery*, 2021, **20**, 101–124.

2 N. G. Lamson, A. Berger, K. C. Fein and K. A. Whitehead, *Nat. Biomed. Eng.*, 2020, **4**, 84–96.

3 Y. Liu, J. Hardie, X. Zhang and V. M. Rotello, *Semin. Immunol.*, 2017, **34**, 25–32.

4 T.-O. Peulen and K. J. Wilkinson, *Environ. Sci. Technol.*, 2011, **45**, 3367–3373.

5 E. C. Cho, Q. Zhang and Y. Xia, *Nat. Nanotechnol.*, 2011, **6**, 385–391.

6 S. E. Skrabalak, J. Chen, Y. Sun, X. Lu, L. Au, C. M. Cobley and Y. Xia, *Acc. Chem. Res.*, 2008, **41**, 1587–1595.

7 C. Sun, J. S. H. Lee and M. Zhang, *Adv. Drug Delivery Rev.*, 2008, **60**, 1252–1265.

8 Y.-C. Yeh, B. Creran and V. M. Rotello, *Nanoscale*, 2012, **4**, 1871–1880.

9 D. P. Linklater, V. A. Baulin, X. L. Guével, J.-B. Fleury, E. Hanssen, T. H. P. Nguyen, S. Juodkazis, G. Bryant, R. J. Crawford, P. Stoodley and E. P. Ivanova, *Adv. Mater.*, 2020, **32**, 2005679.

10 Y. Cao, J. Wang, Q.-Y. Jiang, L. Hu, Y.-J. Yu, Y.-F. Yu and F. Chen, *Nanotheranostics*, 2020, **4**, 201–209.

11 S. Sloan-Dennison and Z. D. Schultz, *Chem. Sci.*, 2018, **10**, 1807–1815.

12 G. H. Weiss and R. J. Rubin, *Advances in Chemical Physics*, John Wiley & Sons, Ltd, 1982, pp. 363–505.

13 V. E. Debets, L. M. C. Janssen and A. Šarić, *Soft Matter*, 2020, **16**, 10628–10639.

14 K. M. Spillane, J. Ortega-Arroyo, G. de Wit, C. Eggeling, H. Ewers, M. I. Wallace and P. Kukura, *Nano Lett.*, 2014, **14**, 5390–5397.

15 Y. Yu, Y. Gao and Y. Yu, *ACS Nano*, 2018, **12**, 11871–11880.

16 Y.-H. Liao, C.-H. Lin, C.-Y. Cheng, W. C. Wong, J.-Y. Juo and C.-L. Hsieh, *ACS Nano*, 2019, **13**, 10918–10928.

17 S. Block, V. P. Zhdanov and F. Höök, *Nano Lett.*, 2016, **16**, 4382–4390.

18 P. Kukura, H. Ewers, C. Müller, A. Renn, A. Helenius and V. Sandoghdar, *Nat. Methods*, 2009, **6**, 923–927.

19 M. J. Saxton, *Biophys. J.*, 2012, **103**, 2411–2422.

20 H. L. E. Coker, M. R. Cheetham, D. R. Kattnig, Y. J. Wang, S. Garcia-Manyes and M. I. Wallace, *Biophys. J.*, 2019, **116**, 1085–1094.

21 M. J. Saxton, *Biophys. J.*, 1987, **52**, 989–997.

22 H. Berry and H. Chaté, *Phys. Rev. E: Stat., Nonlinear, Soft Matter Phys.*, 2014, **89**, 022708.

23 C. Manzo, J. A. Torreno-Pina, P. Massignan, G. J. Lapeyre, M. Lewenstein and M. F. Garcia Parajo, *Phys. Rev. X*, 2015, **5**, 011021.

24 A. V. Weigel, B. Simon, M. M. Tamkun and D. Krapf, *Proc. Natl. Acad. Sci. U. S. A.*, 2011, **108**, 6438–6443.

25 M. V. Chubynsky and G. W. Slater, *Phys. Rev. Lett.*, 2014, **113**, 098302.

26 B. Wang, S. M. Anthony, S. C. Bae and S. Granick, *Proc. Natl. Acad. Sci. U. S. A.*, 2009, **106**, 15160–15164.

27 M. Mahmoudi, I. Lynch, M. R. Ejtehadi, M. P. Monopoli, F. B. Bombelli and S. Laurent, *Chem. Rev.*, 2011, **111**, 5610–5637.

28 P. d. Pino, B. Pelaz, Q. Zhang, P. Maffre, G. U. Nienhaus and W. J. Parak, *Mater. Horiz.*, 2014, **1**, 301–313.

29 C. Gunawan, M. Lim, C. P. Marquis and R. Amal, *J. Mater. Chem. B*, 2014, **2**, 2060–2083.

30 F. Giulimondi, L. Digiacomo, D. Pozzi, S. Palchetti, E. Vulpis, A. L. Capriotti, R. Z. Chiozzi, A. Laganà, H. Amenitsch, L. Masuelli, G. Peruzzi, M. Mahmoudi, I. Screpanti, A. Zingoni and G. Caracciolo, *Nat. Commun.*, 2019, **10**, 3686.

31 P. C. Ke, S. Lin, W. J. Parak, T. P. Davis and F. Caruso, *ACS Nano*, 2017, **11**, 11773–11776.

32 X. l. Guével, F. Palomares, M. J. Torres, M. Blanca, T. D. Fernandez and C. Mayorga, *RSC Adv.*, 2015, **5**, 85305–85309.

33 P. Heo, S. Ramakrishnan, J. Coleman, J. E. Rothman, J.-B. Fleury and F. Pincet, *Small*, 2019, **15**, 1900725.

34 M. Hu, C. Novo, A. Funston, H. Wang, H. Staleva, S. Zou, P. Mulvaney, Y. Xia and G. V. Hartland, *J. Mater. Chem.*, 2008, **18**, 1949–1960.

35 J.-B. Fleury, M. Werner, X. L. Guével and V. A. Baulin, *J. Colloid Interface Sci.*, 2021, **603**, 550–558.

36 R. Wu, H. Peng, J.-J. Zhu, L.-P. Jiang and J. Liu, *Front. Chem.*, 2020, **8**, 121.

37 V. Vallaeys, R. C. Tyson, W. D. Lane, E. Deleersnijder and E. Hanert, *J. R. Soc., Interface*, 2017, **14**, 20160889.

38 E. Porret, L. Sancey, A. Martín-Serrano, M. I. Montañez, R. Seeman, A. Yahia-Ammar, H. Okuno, F. Gomez, A. Ariza, N. Hildebrandt, J.-B. Fleury, J.-L. Coll and X. Le Guével, *Chem. Mater.*, 2017, **29**, 7497–7506.

39 J. Piella, N. G. Bastús and V. Puntes, *Bioconjugate Chem.*, 2017, **28**, 88–97.

40 Y. Guo, E. Terazzi, R. Seemann, J. B. Fleury and V. A. Baulin, *Sci. Adv.*, 2016, **2**, e1600261.

41 F. Fang, J. Satulovsky and I. Szleifer, *Biophys. J.*, 2005, **89**, 1516–1533.

42 P. Hänggi, P. Talkner and M. Borkovec, *Rev. Mod. Phys.*, 1990, **62**, 251–341.

43 J.-B. Fleury and V. A. Baulin, *Proc. Natl. Acad. Sci. U. S. A.*, 2021, **118**(31), e2104610118.

44 D. Allan, C. van der Wel, N. Keim, T. A. Caswell, D. Wieker, R. Verweij, C. Reid, T. L. Grueter, K. Ramos, A. Zoeith, R. W. Perry, F. Boulogne, P. Sinha, P. N. Bruot, L. Uieda, J. Katins, H. Mary and A. Ahmadia, *soft-matter/trackpy: Trackpy v0.4.2, 2019*, https://zenodo.org/record/3492186#.YD-bSWhKiUk.

45 J. T. Hynes, *Annu. Rev. Phys. Chem.*, 1977, **28**, 301–321.

46 P. E. Jahl and R. Parthasarathy, *Assessing the use of ellipsoidal microparticles for determining lipid membrane viscosity*, 2021.

47 S. V. Koniakhin, I. E. Eliseev, I. N. Terterov, A. V. Shvidchenko, E. D. Eidelman and M. V. Dubina, *Microfluid. Nanofluid.*, 2015, **18**, 1189–1194.

48 G. J. Amador, D. van Dijk, R. Kieffer, M.-E. Aubin-Tam and D. Tam, *Proc. Natl. Acad. Sci. U. S. A.*, 2021, **118**, e2100156118.

49 T. T. Hormel, S. Q. Kurihara, M. K. Brennan, M. C. Wozniak and R. Parthasarathy, *Phys. Rev. Lett.*, 2014, **112**, 188101.

50 H. A. Faizi, R. Dimova and P. M. Vlahovska, *Viscosity of fluid membranes measured from vesicle deformation*, 2021.

51 G. Campagnola, K. Nepal, B. W. Schroder, O. B. Peersen and D. Krapf, *Sci. Rep.*, 2015, **5**, 17721.

52 V. V. Palyulin, G. Blackburn, M. A. Lomholt, N. W. Watkins, R. Metzler, R. Klages and A. V. Chechkin, *New J. Phys.*, 2019, **21**, 103028.

53 *Lévy Processes and Stochastic Calculus*, ed. D. Applebaum, Cambridge University Press, Cambridge, 2nd edn, 2009, pp. 1–81.

54 E. Bouchaud and M. Daoud, *J. Phys. A: Math. Gen.*, 1987, **20**, 1463–1470.

55 M. S. Abe, *Proc. Natl. Acad. Sci. U. S. A.*, 2020, **117**, 24336–24344.

56 M. Nygaard, B. B. Kragelund, E. Papaleo and K. Lindorff-Larsen, *Biophys. J.*, 2017, **113**, 550–557.

57 H. Larsericsdotter, S. Oscarsson and J. Buijs, *J. Colloid Interface Sci.*, 2005, **289**, 26–35.

58 W. Wang, Z. Huang, Y. Li, W. Wang, J. Shi, F. Fu, Y. Huang, X. Pan and C. Wu, *Acta Pharm. Sin. B*, 2021, **11**, 1030–1046.

59 S. D. Perrault and W. C. W. Chan, *J. Am. Chem. Soc.*, 2009, **131**, 17042–17043.

60 S. Puza, S. Caesar, C. Poojari, M. Jung, R. Seemann, J. S. Hub, B. Schrul and J.-B. Fleury, *Small*, 2022, 2106524.

61 J.-B. Fleury, *RSC Adv.*, 2020, **10**, 19686–19692.

62 K. L. Johnson, K. Kendall, A. D. Roberts and D. Tabor, *Proc. R. Soc. London, Ser. A*, 1971, **324**, 301–313.

63 G. Volpe and G. Volpe, *Am. J. Phys.*, 2013, **81**, 224–230.